Correlations between structure and electrical properties of Cr-Ta thin films prepared by oblique angle co-sputtering

Hamidreza Gerami[1], Guillem Vilar Soler[2], Jean-Marc Cote[1], Jean-Baptiste Sanchez[2], Nicolas Martin[1, *]

[1] Université Marie et Louis Pasteur, SUPMICROTECH, CNRS, Institut FEMTO-ST, 25000 Besançon Cedex, France

[2] Université Marie et Louis Pasteur, CNRS, Institut FEMTO-ST, 25000 Besançon Cedex, France

[*] Author to whom correspondence should be addressed: nicolas.martin@femto-st.fr.

Highlights

- Cr-Ta thin films are produced by GLAD co-sputtering.
- Column tilt angle and composition can be tuned playing with Cr and Ta target currents.
- Between 7 and 300 K, resistivity *vs.* temperature exhibit a metallic-like behaviors.
- A crossover temperature is defined due to electron-phonon-defect interactions.
- The crossover temperature is connected to composition and Debye temperature of Cr and Ta.

Graphical abstract

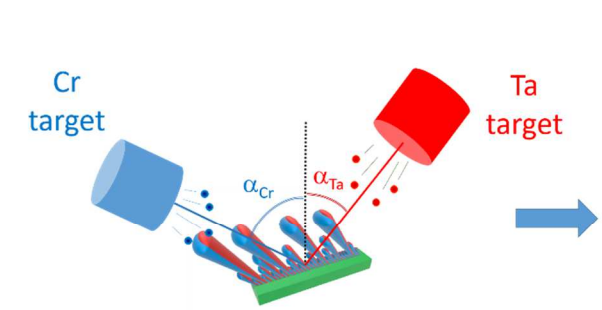

Tunable [Cr] and [Ta] playing with target currents

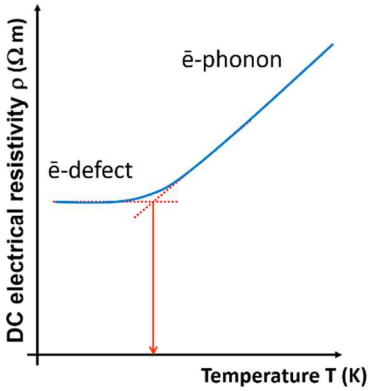

Crossover temperature = f([Cr] and [Ta])

Abstract:

Cr-Ta thin films were deposited on glass and (100) silicon substrates by DC magnetron co-sputtering. Films were prepared by the glancing angle deposition (GLAD) method by fixing the deposition angle to 80° for both targets. The Cr and Ta target currents were systematically and reversely changed from 0 mA to 300 mA, so as to tune the composition of the films. All other working parameters were kept constant. For such GLAD co-sputtering conditions, the deposition time was adjusted in order to get a film thickness close to 400 nm. A columnar microstructure was obtained with a Janus-like architecture as a function of the operating target currents. Different morphologies and tilted column angles were produced by adjusting target currents. The typical hexagonal Cr phase was produced for Cr-rich films, whereas a mixture of α and β-Ta phases for Ta-rich films. DC electrical resistivity *vs*. temperature showed the typical metallic-like behaviors for all Cr-Ta films. The electron-phonon and electron-defect interactions were investigated, and correlated with variations of the film's composition and structure.

Keywords: Glancing Angle Deposition, Co-sputtering, Cr-Ta Films, Resistivity, Crossover Temperature.

1. Introduction

Thin films deposition by co-sputtering allows tuning composition, structure and thus many physico-chemical properties [1-3]. An abundant literature has been produced these last decades about the growth of original coatings (multilayers, graded compositions, phase mixture, …) implementing this strategy of co-deposition processes. Although such approach allows fabricating various compounds and alloys, tuning the shape of the columnar structure appears as a challenging task and can be achieved by means of post-deposition treatments or by the development of new deposition processes such as the GLancing Angle deposition (GLAD) technique [4-6]. Since 1995, the Brett's team particularly acted as a pioneer for expanding the potential of this technique, and thus they strongly contributed to demonstrate the extended properties of GLAD films [7]. As a result, many other groups have adopted the GLAD strategy for fabricating various columnar architectures (tilted columns, zigzags, helices and so on) [8-12]. However, the greater part of studies has reported thin films prepared with a vacuum process involving a single particle source. If the single source technique provides exciting opportunities for the structural design of thin films on the sub-micrometer scale by controlling substrate angle and rotation, the two sources process extends even more the capabilities of the GLAD approach to further engineer these columnar architectures and so, the film properties [13, 14].

Several material combinations have been studied by different co-sputtering systems using tilted and focused targets [15-20]. These former investigations implement deposition configurations which do not strictly correspond to a glancing angle geometry of the incoming particle fluxes since targets are inclined with angles no more than a few tenths of degrees compared to the normal of the substrate surface. One can therefore suggests that the co-deposition GLAD sputtering process turns out to be more interesting when targets are tilted with angles higher than 70° since the shadowing effect become efficient and is considered as

the driving force of the thin film growth mechanism. For such operating conditions, very few studies report on the deposition of thin films involving to nearly facing sputtered targets [21-23]. Zhou *et al.* [24] successfully produced Ta-Si nanostructures exhibiting vertically oriented, or zigzag columns with alternating Ta and Si elements, or even mosaic-like features by simultaneously depositing these two elements. Later, other authors prepared Janus-like columns of Ti-Ag [25], W-Cu [26], W-Mo [27] or W-Ag [28] thin films, or even W-Mo chequerboard-like structure [29] by GLAD co-sputtering with nearly facing targets (angle of 80° for both targets). It was clearly shown that the columnar architecture, the chemical composition of the films, and thus the resulting properties can be tailored playing on the sputtering current of each target. It is also worth of noting that when the sputtered particles are mainly in ballistic regime (argon pressure much lower than 1 Pa), the GLAD co-sputtering configuration does not only lead to create bicomponent columns, but it also becomes a relevant tool to favor the growth of anisotropic columnar cross-sections (elliptical shape in the direction perpendicular to the particle fluxes), and thus a way to produce thin films with anisotropic behaviors relevant in wave propagation [30] or electronic transport properties [31]. It was clearly shown that for some metallic GLAD thin films such as W, the directional dependence of electrical resistivity and elastic wave propagation is closely related to the anisotropic structural characteristics of the tilted columnar structure (fanning of the cross-section). The authors also demonstrated that this anisotropy can be improved due to an enhancement of the anisotropic structure, especially in Janus-like W-Cu architecture after a chemical etching of Cu.

In this paper, we report on the GLAD co-deposition of Cr-Ta thin films. Cr and Ta targets are simultaneously sputtered using the same deposition angle of 80° in order to be in a glancing angle configuration. The choice of Cr and Ta metals is based-on their Debye temperature (240 K and 630 K for Ta and Cr, respectively). For single metals, this Debye temperature is closely related to the evolution electrical resistivity *vs.* temperature (especially

at a few tens of K) where a crossover temperature correlates with interferences between electron-phonon and electron-defect interactions [32]. When two different metals are co-sputter-deposited by GLAD, some original designs (Janus-like structure) can be produced. However, a few studies can be found in the literature implementing the deposition of these two components columnar thin films, and to the best of our knowledge, electronic transport properties of such GLAD bimetallic columnar films at very low temperature have never been reported. As a result, combining of Cr and Ta metals inside the tilted columnar structure by means of GLAD co-sputtering correspond to a twofold objective. It is thus shown that the crossover temperature of Cr-Ta films is closely connected to the metal concentration. To this end, current intensities applied to each target are taken as key parameters to tune the chemical composition, the columnar structure and so, electronic transport properties of Cr-Ta films.

2. Experimental details

In the present work, Cr-Ta thin films were co-deposited onto glass and (100) silicon substrates. A home-made DC magnetron sputtering system was developed involving metallic targets with a purity of 99.95% and a diameter of 51 mm (more details can be found in [27]). Briefly, the deposition took place in a 40 L vacuum chamber, which was evacuated using a turbomolecular pump backed by a primary pump, resulting in a residual pressure lower than 10^{-5} Pa. The distance between the substrate center and the target center was 65 mm from top target (Cr) and 95 mm from bottom target (Ta). Sputtering was conducted in a pure argon atmosphere, with a flow rate of 2.6 sccm and a constant pumping speed of 13 L s^{-1}, leading to an argon sputtering pressure of 0.3 Pa. Thin films were prepared by the glancing angle co-deposition method by fixing the deposition angle to $\alpha_{Cr} = \alpha_{Ta} = 80°$ for both targets (Fig. 1).

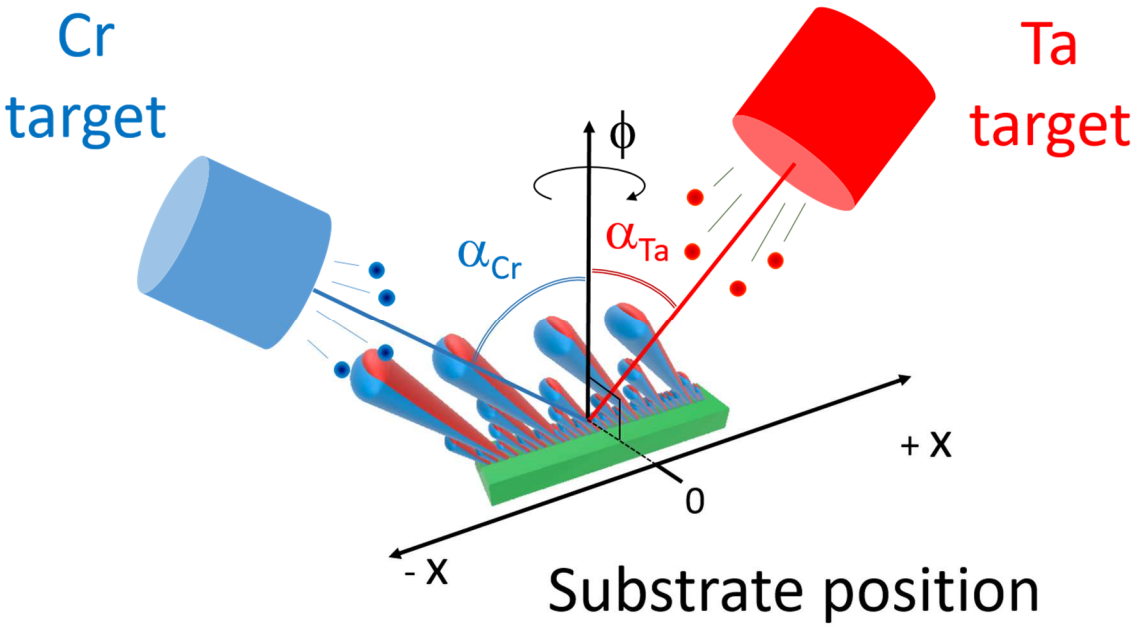

Figure 1: Schematic representation of the oblique angle co-sputtering system implemented to deposit Cr-Ta thin films. Each target is tilted with the same deposition angle, *i.e.*, $\alpha_{Cr} = \alpha_{Ta} = 80°$. The target-to-substrate distances are maintained at 65 mm for Cr and 95 mm for Ta. The substrate is fixed (no rotation following ϕ angle) and both targets are focused on the center of the substrate position ($x = 0$ mm).

Cr and Ta target currents, namely I_{Cr} and I_{Ta}, respectively, were systematically and reversely changed from 0 mA to 300 mA following at least 7 different currents. For all co-sputtering conditions, the deposition time was adjusted in order to get a film thickness close to 400 nm at the center of the substrate ($x = 0$ mm). Substrates remained grounded throughout the process, with no external heating applied. Prior to deposition, they were ultrasonically cleaned using acetone and ethanol (analytical grade).

Structural analyses were performed on films deposited on silicon substrates. The surface and cross-sectional morphology were examined using a JEOL JSM 7600F scanning electron microscope (SEM). The chemical composition was determined by energy-dispersive X-ray spectroscopy (EDX). The atomic concentrations of Cr and Ta were analyzed for 7 different positions on the sample following the direction of the particle fluxes ($-x$ to $+x$). The

crystallographic structure was characterized using X-ray diffraction (XRD) with a PAnalytical Aeris diffractometer, employing a copper X-ray source (Cu $\lambda_{K\alpha 1,2}$ = 0.15418 nm) in a grazing incidence configuration (GIXRD) with an X-ray incidence angle of θ = 0.8°. The scans were conducted over a 2θ range of 20° to 90° with a step size of 0.02° per second. DC electrical resistivity measurements were performed on films deposited onto glass substrates, spanning a temperature range from 7 K to 300 K, using the four-probe van der Pauw method. A cryostat system (ARS cryocooler series CS-204-AE from Advanced Research Systems) was used to cool the samples down to approximately 6 K in a vacuum chamber maintained below 10^{-4} Pa. A temperature ramp of 1 K per minute was applied during all resistivity measurements.

3. Results and discussion

3.1. Morphology, structure and composition

Top and cross-section SEM views of Cr-Ta thin films are shown in Fig. 2. A columnar micro-structure is typically observed with a column orientation depending on Cr and Ta target currents. For the highest Cr currents, films are more porous with a voided architecture between tilted columns. The latters are better defined and more separated for these operating conditions. In addition, column angle is orientated following a direction facing the Cr target. Assuming that the sputtering yield of Cr is higher than that of Ta and due to the shorter substrate-to-target distance (65 mm for Cr against 95 mm for Ta), one can expected inclined columns in the direction of Cr target even for unbalanced target currents, *i.e.*, $I_{Cr} < I_{Ta}$.

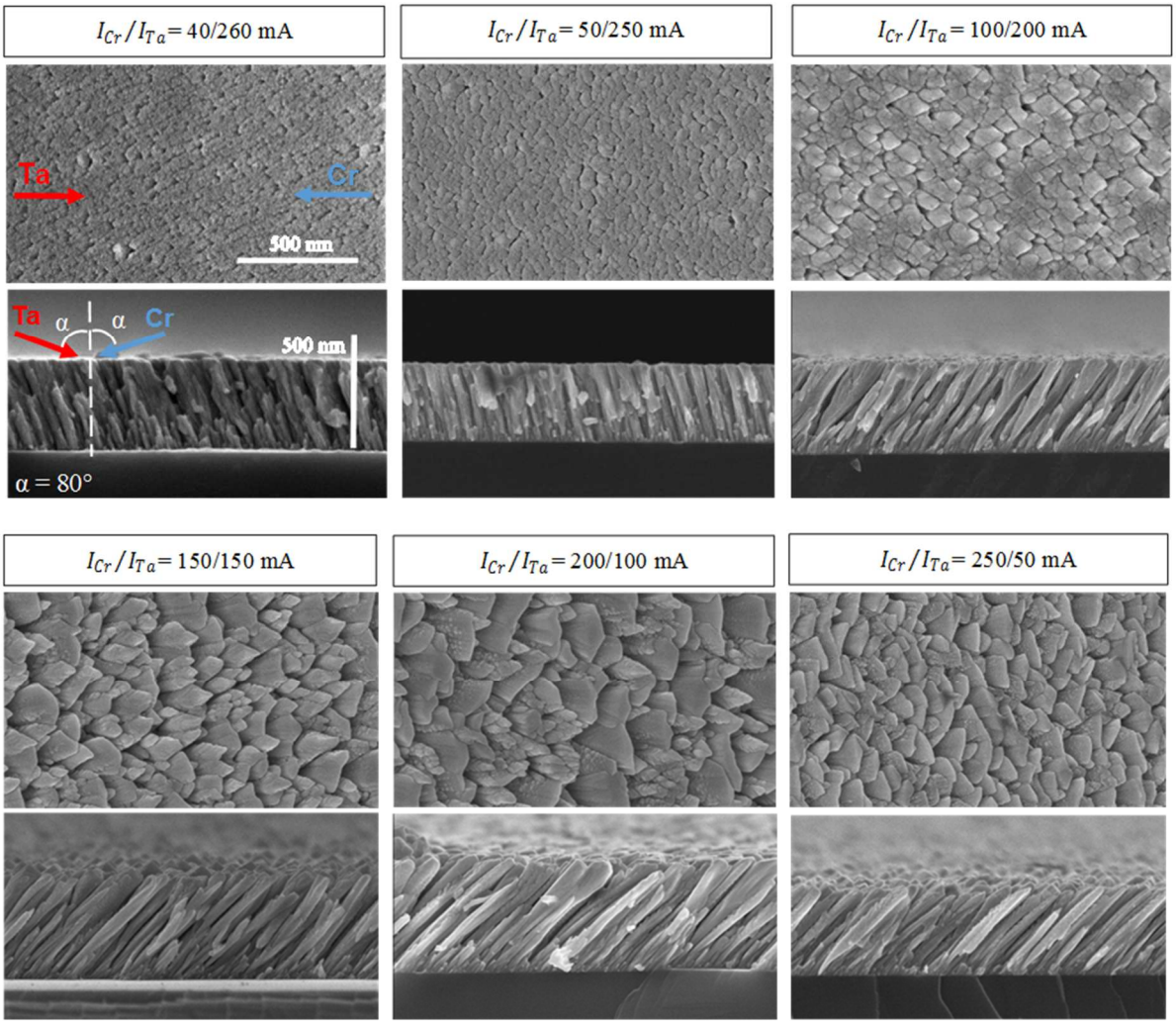

Figure 2: Scanning electron microscopy (SEM) observations of top and cross-section views of co-deposited Cr-Ta films with various Cr and Ta target currents (I_{Cr}/I_{Ta}). They are systematically and inversely changed from 0 to 300 mA. Column apexes and tilts can be adjusted as a function of both target currents. Arrows indicate the incoming of Cr (blue) and Ta (red) particle fluxes.

As a result, assuming the geometry of the GLAD co-deposition system and the operating parameters, the growth of Cr predominantly influences and controls the growth the columnar structure for co-sputtering until around I_{Cr} = 60 mA and I_{Ta} = 240 mA. This behavior is driven by two factors: First, the operating conditions such as target currents and target-to-substrate distance, which favor the Cr flux in comparison to that of Ta; Second, Cr exhibits a higher deposition rate due to a shorter target-to-substrate distance and a higher sputtering yield than

Ta. In other words, changing at the same time and reversely currents of both targets from I_{Cr}/I_{Ta} = 300/0 mA to I_{Cr}/I_{Ta} = 0/300 mA easily allows playing with the columns orientation from Cr to Ta side.

Precisely adjusting both target currents can also lead to the growth of columns perpendicular to the substrate surface. As a first approximation, plotting column angle *vs.* I_{Cr}; I_{Ta} and supposing a continuous evolution of column angle with target currents, interpolation gives rise to normal columns for I_{Cr} = 67 mA and I_{Ta} = 233 mA (Fig. S1 in Supplementary Material). Note that these target current values where the columns growth is normal to the susbtrate depends on several parameters like metal sputtering yields, sputtering pressure, target-to-substrate distances among others.

Top views by SEM show that the surface morphology of Cr-Ta films is also influenced by the target currents. For I_{Cr} < 50 mA and I_{Ta} > 250 mA, columns are rather connected to each other with apexes poorly defined, size around 50 nm and separated by small voids. Increasing the Cr target current to 100 mA (and so decreasing I_{Ta} to 200 mA) leads to bigger and more distinct columns with a sharped top orientation in the direction of the Cr atom flux. Voids between columns are also better distinguishable. A further increase of I_{Cr} associated to a decrease of I_{Ta} (*e.g.*, I_{Cr}/I_{Ta} = 200/100 mA) produces elongated cross-section columns normally to Cr and Ta particle fluxes. Increasing the Cr current while reducing the Ta one significantly amplifies the atomic shadowing effect, leading to the formation of a distinct porous structure with bigger voids between the columns. This shadowing effect promotes the growth of self-affine columnar nanorods, which develop with a noticeable tilting angle (column angle reaches 46°). On the other hand, bigger and more elliptical shapes of the column cross-sections are obtained for I_{Cr} > 250 mA and I_{Ta} < 50 mA. This is mainly assigned to an anisotropic growth of the columnar structure. It has ever been encoutered in tungsten GLAD films, and closely connected to the low self-diffusion length of W atoms and a high melting point favoring the

shadowing effect [33]. Columns grow along the direction perpendicular to the particle flux giving rise to a fanning of their cross-section. The latter exhibits a crescent-like shape as deposition continues [34]. Columns are connected to each other by chains (normal to the flux) and an anisotropic structure is produced. This structural anisotropy has also been reported for other metallic GLAD films [35] and sometimes emphasizes for deposition angles higher than 60°. It was clearly shown that an anisotropic microstructure is favored as the film's thickness increases. The column cross-section becomes more asymmetric with an elliptical shape perpendicular to the incoming particle flux. This asymmetric shape of the columns directly influences the electronic transport properties and the acoustic wave propagation, both being enhanced in the largest direction of the cross-section. In addition, this anisotropic microstructure was connected to the ballistic character of sputtered particles (high directional flux for a sputtering pressure lower than 0.25 Pa), which promotes the shadowing effect from the first growing stage and during the film growth.

For Cr and Ta metals, the surface self-diffusion energy is very close (1.2 eV from [36]) and cannot be assumed to explain the elliptical shape of the columns cross-section. Since Cr is lighter than Ta and due to the closest target-to-substrate distance (65 nm against 95 mm, respectively), one may suggest that Cr atoms impinging on the growing film with a more thermalized character than Ta atoms [37]. Since there is no shadowing mechanism which restrict the growth perpendicular to the deposition direction, fanning of the columns becomes more significant for Cr-rich columns. In addition, increasing the Cr target current induces the column bundling perpendicularly to the Cr flux and thus the development of an elongated column cross-section.

GIXRD patterns of Cr-Ta films deposited on Si substrates were recorded as a function of the target currents (Fig. 3). For pure Cr films and up to I_{Cr}/I_{Ta} = 200/100 mA, patterns exhibit diffracted signals corresponding to the hexagonal close packed structure (hcp) of the Cr metal

with intense peaks related to (110) and (211) crystallographic planes. Reducing the Cr target current and increasing the Ta one diminishes Cr peaks while broad and small signals appear due to the occurrence of α-Ta phase (body centered cubic structure - bcc).

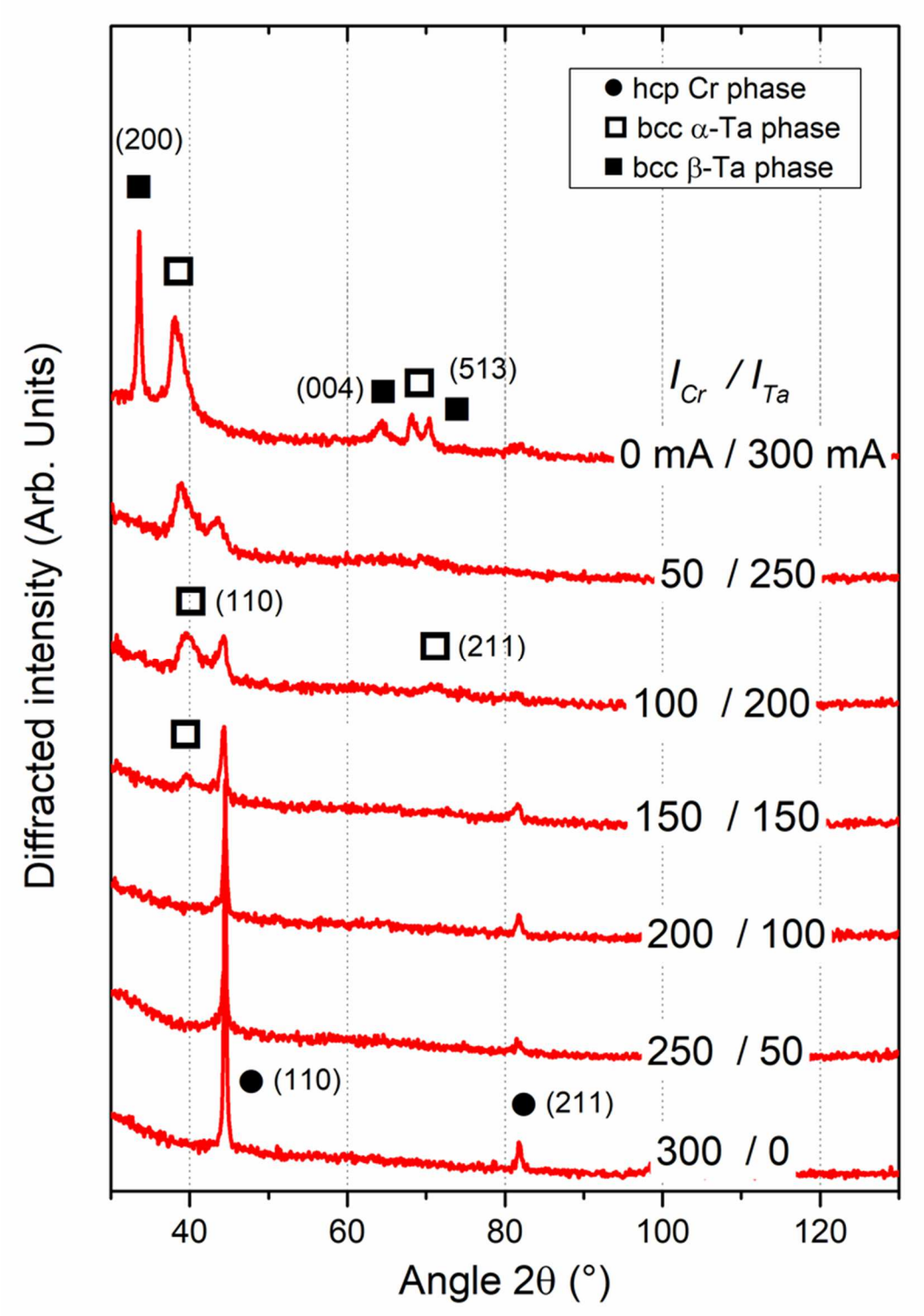

Figure 3: GIXRD patterns of Cr-Ta thin films co-sputter-deposited on glass substrate by oblique angle deposition. Cr and Ta target currents are systematically and inversely changed from 0 to 300 mA. Occurrence of the hcp Cr phase and α and/or β-Ta phases depends on the Cr and Ta target currents.

A further increase/decrease of Cr/Ta target currents develops the poorly crystalline structure of the films although the (110) peak due to α-Ta progresses, but still remains noisy and slightly intense. Therefore, Cr-Ta films prepared with I_{Cr}/I_{Ta} = 50/250 mA (growth of columns nearly normal to the substrate surface from Fig. 2) are poorly crystalline and made of hcp Cr and α-Ta phases with crystal sizes of a few nanometers. It is interesting of remarking that without Cr sputtering (I_{Cr}/I_{Ta} = 0/300 mA), Ta films show a mixture of α- and β-Ta phases. The occurrence of this β-Ta phase (tetragonal structure) has ever been reported by Colin *et al.* [38]. Since the GLAD deposition process produces a porous architecture and defects, metastable phases such as the β-phase in Ta metal can be particularly favored [39]. Due to our operating conditions (deposition angle α = 80°, Ta-to-substrate distance = 95 mm), we may argue that low-energy Ta atoms (most of them are thermalized) arrive on the column apex, which promotes the stability of the β-Ta phase.

Cr and Ta target currents have also an influence on Cr and Ta atomic concentrations in Cr-Ta films. In order to show that tunable compositions can be achieved, Cr and Ta contents were analyzed at seven different *x* positions (from *x* = -6 to +6 mm and every 2 mm) on the sample as referred in figure 1 (Fig. 4). For all Cr and Ta target currents, Cr-to-Ta atomic concentration ratio gradually varies as a function of the *x* position on the samples. When I_{Cr}/I_{Ta} changes from 10/290 to 250/50 mA, the range of ratios spans two orders of magnitude, *i.e.*, from 10^{-1} to more than 3×10^{1}, respectively. As expected, Cr-rich films are obtained for I_{Cr} higher than 100 mA (I_{Ta} lower than 200 mA), whereas an opposite variation of target currents leads to Ta-rich films. Cr and Ta concentrations are equimolar for I_{Cr}/I_{Ta} around 40/260 mA,

which does not correspond to the same Cr and Ta target currents. The target-to-substrate distance is shorter for Cr target and its sputtering yield is higher than that of Ta. So, the Ta target requires a higher sputtering current than Cr target to get equivalent Cr and Ta particle fluxes.

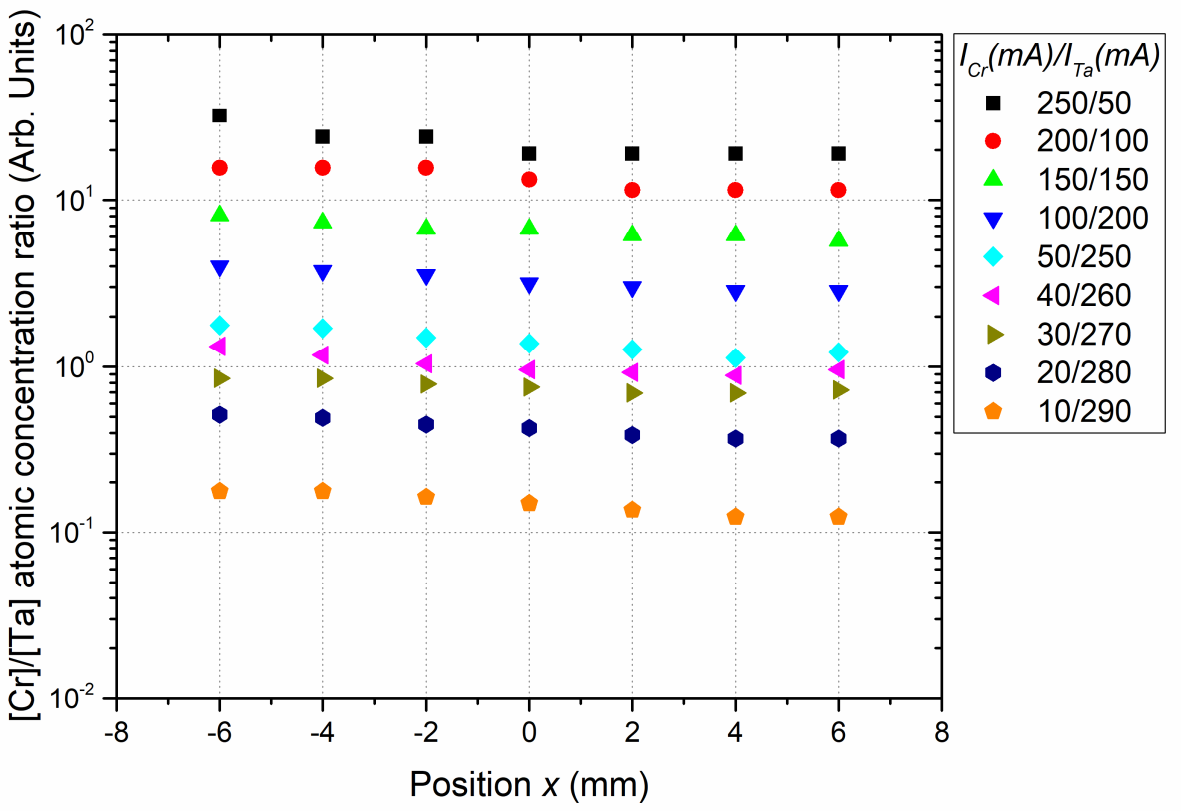

Figure 4: Atomic concentration ratio [Cr]/[Ta] as a function of the position x on the Si(100) substrate and for different current intensities of chromium and tantalum targets. Measurements of the atomic concentration are performed on seven different locations. The center of the substrate corresponds to $x = 0$ mm, $x = -6$ mm is the left-hand side (close to the chromium target) and $x = +6$ mm is the right-hand side (close to the tantalum target). Accuracy of each atomic concentration is ± 0.3 at. % (not shown for clarity).

This gradual and monotonous variation of the films composition *vs.* substrate position has similarly been reported for other bimetallic compounds co-sputter-deposited by GLAD [28, 40]. This gradient of composition depends on the sputtering yield of the metals and current applied to each target. Although Cr and Ta exhibit a significant difference of sputtering yield (1.32 against 0.42 at Ar^+ energy of 300 eV for Cr and Ta, respectively [41]), disparity of atomic

concentration ratios between the two opposite positions on the substrate (x = -6 mm and +6 mm) is in the range of a few at. %. In order to better illustrate the effect of Cr and Ta target currents on Cr-Ta films composition, the atomic concentration of both metals taken at the center of the substrate position (x = 0 mm) is plotted as a function of I_{Cr} and I_{Ta} (Fig. 5).

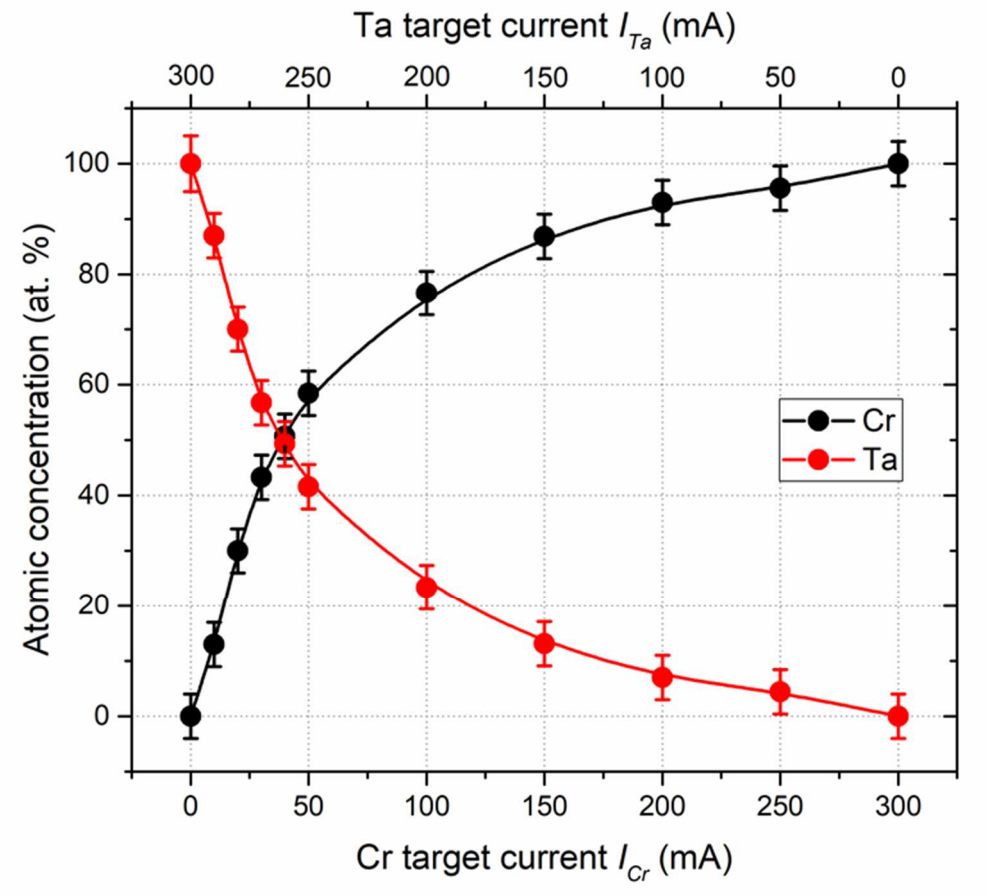

Figure 5: Cr and Ta atomic concentrations as a function of Cr and Ta target currents of 400 nm thick Cr-Ta thin films co-sputter-deposited by GLAD on Si(100). A symmetric, reverse and continuous evolution of each metal concentration is produced with equimolar films obtained for I_{Cr} = 40 mA and I_{Ta} = 260 mA.

Both metal concentrations exhibit a continuous but non-linear evolution *vs.* target currents. Because of the shorter target-to-substrate distance and higher sputtering yield, Cr concentration rapidly increases from 0 to 50 at. % as I_{Cr} changes from 0 to 50 mA. On the other hand, Ta concentration varies only of a few at. % as I_{Ta} rises with the same range. Plotting Cr and Ta contents *vs.* I_{Cr}/I_{Ta} also points out the determination of an equimolar composition in Cr-

Ta films for I_{Cr}/I_{Ta} = 40/260 mA (likewise confirmed from XPS analyses as shown in Fig. S2 in Supplementary Material). It is also worth noticing that these operating conditions do not necessarily correspond to the growth of columns normal to the substrate surface as shown from SEM observations in figure 2 (interpolation gave rise to perpendicular columns for I_{Cr} = 70 mA and I_{Ta} = 230 mA).

3.2. Electronic transport properties

DC electrical resistivity ρ as a function of temperature T was measured from 7 to 300 K for all Cr-Ta films sputter-deposited on glass substrate and for different I_{Cr}/I_{Ta} target currents (Fig. 6).

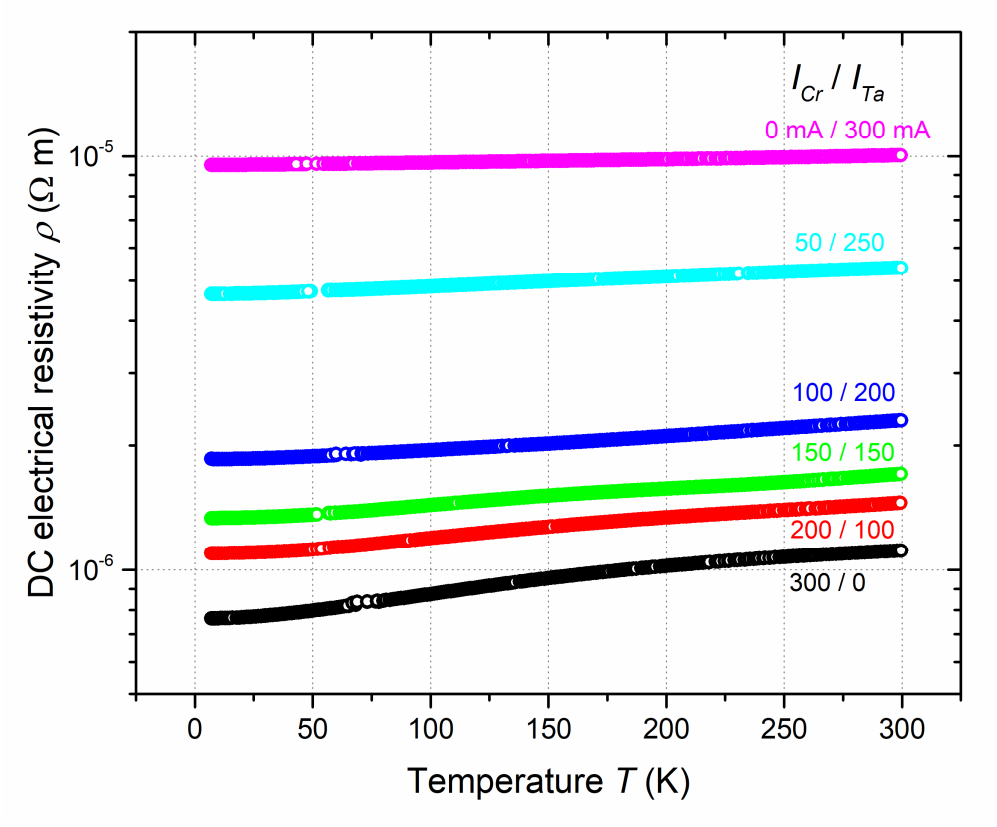

Figure 6: DC electrical resistivity ρ *vs.* temperature T of Cr-Ta thin films sputter-deposited on glass. Cr and Ta target currents I_{Cr} and I_{Ta}, are systematically and reversely changed from 0 to 300 mA. I_{Cr}/I_{Ta} = 300/0 mA corresponds to pure Cr film, whereas I_{Cr}/I_{Ta} = 0/300 mA relates to pure Ta film.

A typical metallic-like behavior is obtained for all samples. A linear evolution of ρ *vs.* T is measured for temperatures down to a few tens of K. This linear variation is usually observed in metallic polycrystalline thin films. Such a temperature dependence of the electrical resistivity is assigned to the electron-phonon interaction. Decreasing even more the temperature (lower than about 15 K) the metal resistivity becomes constant and gives rise to the residual resistivity of the sample, namely ρ_o, and later taken at 7 K (*i.e.*, $\rho_o = \rho_{7K}$ as a first approach). The latter is temperature independent and is due to electron scattering by defects. It is also worth noting that at room temperature, resistivity is in the range 10^{-6} to 10^{-5} S m^{-1}, which is significantly higher than the bulk metal values (close to 10^{-8} S m^{-1} for most metals). Although more resistive compounds are usually obtained when deposited as thin films due to their polycrystalline structure and small grain sizes, resistivity does not go over 10^{-6} S m^{-1} for conventional films (sputtering with deposition angle $\alpha = 0°$). Because of the high voided architecture obtained by the oblique angle deposition process, electron scattering is favored which reduces the conducting behavior of metallic thin films. Oblique angle co-sputtering produces even more growing defects and a phases mixture (as shown from GIXRD in Fig. 3) reducing the electron mean free path and so leading to a low conductive material.

For a given temperature (*e.g.*, 300 K), Cr-Ta films resistivity ρ_{CrTa} *vs.* composition may follow a linear evolution and so a simple rule of mixtures can be assumed following [27]:

$$\rho_{CrTa} = x_{Cr} \times \rho_{Cr} + x_{Ta} \times \rho_{Ta} \quad (1)$$

Where x_{Cr} and x_{Ta} are the Cr and Ta atomic fractions (arb. units), respectively, and ρ_{Cr} and ρ_{Ta} the resistivity of Cr and Ta (Ω m), respectively (resistivities due to electron-phonon interactions and electron scattering by crystal defects are neglected). The linear interpolation of ρ_{CrTa} *vs.* x_{Ta} gives rise to $\rho_{Cr} = 7.67\times10^{-7}$ Ω m and $\rho_{Ta} = 1.01\times10^{-5}$ Ω m with a good agreement between fitting according to a rule of mixtures and experimental data (Fig. S3 in Supplementary Material). These resistivity values of Cr and Ta obtained at x_{Cr} =0 and x_{Ta} =0, respectively, are

a few orders of magnitude higher than that of bulk materials, which is assigned to the porous structure and the high concentration of defects in GLAD films.

Scattering mechanisms of electrons in GLAD thin films can be more discussed from resistivity *vs.* temperature measurements, particularly at low temperature where the electron-phonon and electron-defect interactions compete to each other. These interactions are thoroughly analyzed by focusing on the evolution of resistivity in the temperature range around 0.1×θ, *i.e.*, in-between 10-100 K for most of elementary metals (θ is the Debye temperature of the metal). Based-on the intersection between $(d\rho/dT)_{100K}$ and residual resistivity ρ_{7K} taken at 7 K, a crossover temperature T_{Cr} can be defined as shown as an example in Fig. 7 for a Cr-Ta film prepared with I_{Cr}/I_{Ta} = 200/100 mA with T_{Cr} = 44 K.

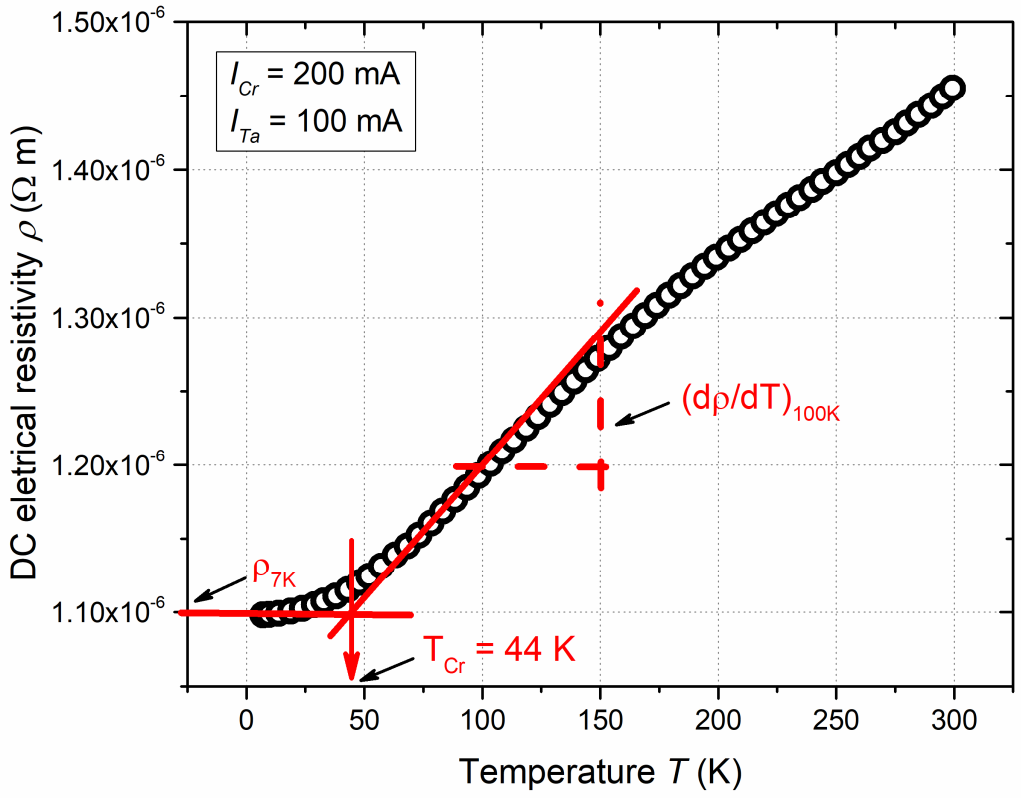

Figure 7: Resistivity *vs.* temperature of a Cr-Ta film prepared by oblique angle co-sputtering with I_{Cr} = 200 mA and I_{Ta} = 100 mA. The crossover temperature T_{Cr} = 44 K representing the transition from *T*-linear to T^5 behavior is determined taking into account the intersection between the residual resistivity (resistivity value at 7 K, namely ρ_{7K}, which is temperature independent), and the derivative of the resistivity by temperature at 100 K, $(d\rho/dT)_{100K}$.

The crossover temperature has been determined for all Cr-Ta films and plotted as a function of the Cr and Ta target currents (Fig. 8a) and [Cr]/[Ta] atomic concentration ratio (Fig. 8b).

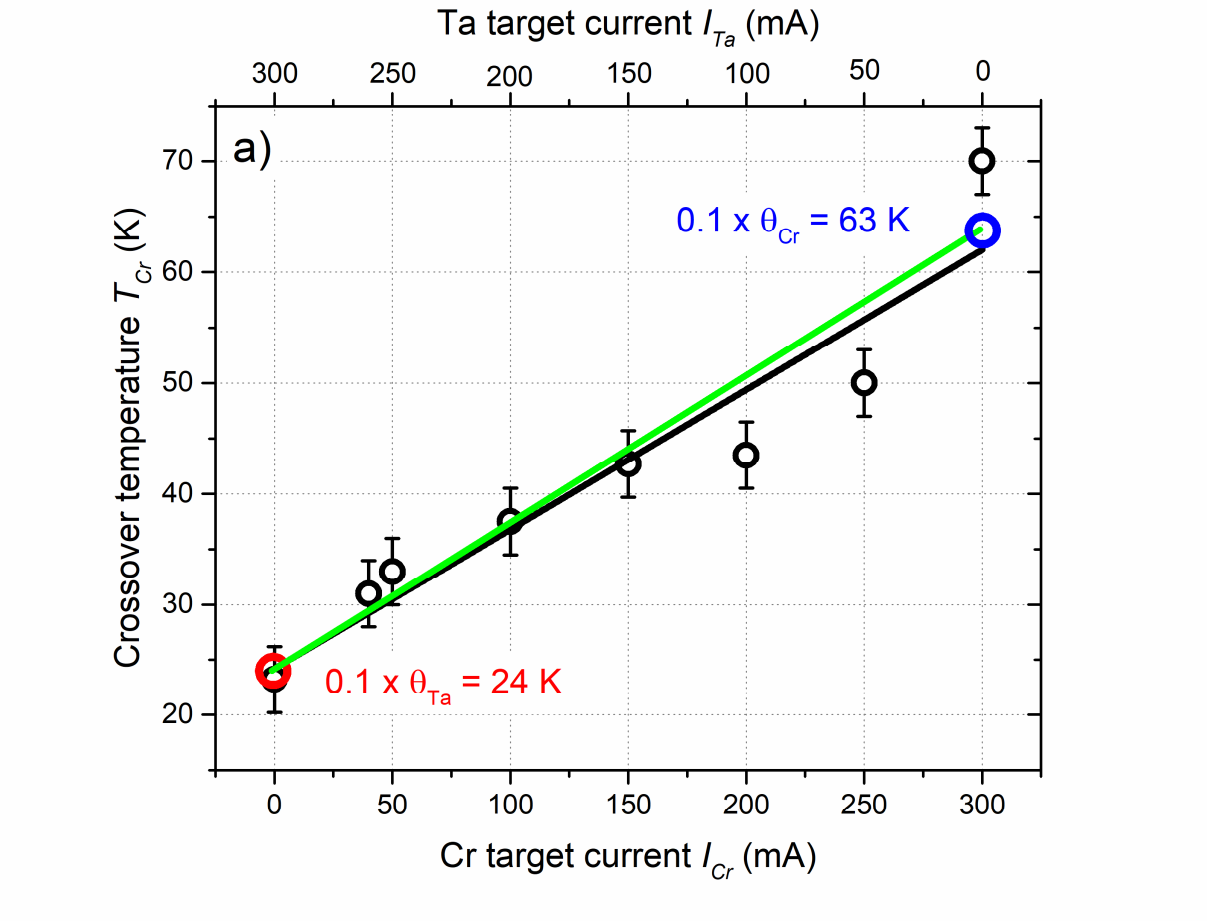

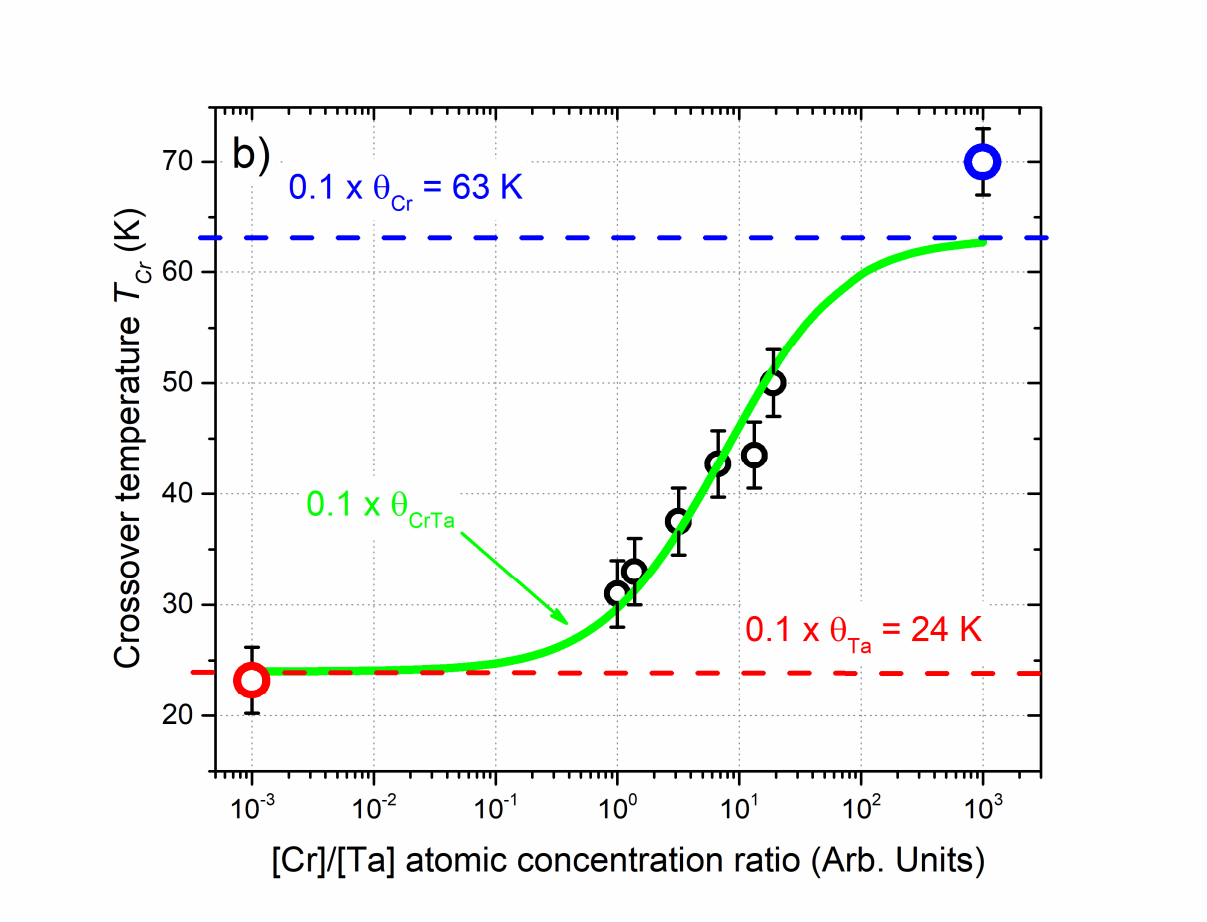

Figure 8: a) Crossover temperature T_{Cr} as a function of Cr and Ta target currents I_{Cr} and I_{Ta}, respectively. Cr and Ta Debye temperatures, namely θ_{Cr} and θ_{Ta}, respectively, are also indicated. Green solid line is a plot from equation (2) of the crossover temperature T_{Cr} *vs.* target current I_{Cr} assuming $0.1\times\theta_{Cr}$ and $0.1\times\theta_{Ta}$ as boundaries for pure Cr (I_{Cr}/I_{Ta} = 300/0 mA) and Ta (I_{Cr}/I_{Ta} = 0/300 mA). Black solid line is a linear fit from experimental crossover temperatures. b) Evolution of the crossover temperature T_{Cr} as a function of Cr-to-Ta atomic concentration ratio. Blue dashed line is $0.1\times\theta_{Cr}$, red dashed line is $0.1\times\theta_{Ta}$, and green line is one-tenth of Debye temperature $\theta_{Cr\text{-}Ta}$ of Cr-Ta films calculated from equation (6).

At first, a linear interpolation (black solid line in Fig. 8a) can be reasonably applied from experimental crossover temperature obtained from different Cr (and Ta) target currents. Similarly, the crossover temperature T_{Cr} can be expressed as a linear evolution as a function of the Cr target current I_{Cr} following:

$$T_{Cr} = A \times I_{Cr} + B \qquad (2)$$

where

$$A = \frac{\theta_{Cr} - \theta_{Ta}}{10\left(I_{Cr}^{Max} - I_{Cr}^{min}\right)} \quad (3)$$

$$B = \frac{\theta_{Ta}}{10} \quad (4)$$

Equation (2) is plotted in figure 8a (green solid line). The discrepancy between these two linear behaviors is rather small. This proves that the crossover temperature corresponding to interferences between electron-phonon and electron-defect interactions can be accurately determined knowing only the Debye temperature of elementary metals and target currents. Little disagreements can be noticed for Cr-rich Cr-Ta films where experimental crossover temperatures as well as the two linear fits exhibit some deviations. They may be assigned to some errors induced by the experimental determination of the crossover temperature, especially for GLAD Cr films, which exhibit a minimum resistivity at temperature around 50 K [32]. Depositing at glancing angle leads to a shift towards higher temperature and the range of temperatures where interferences of electron-pho

non-defect interactions occur is somewhat around 0.15×θ.

Knowing the composition of Cr-Ta films, the Kopp-Neumann relation was applied to calculated their Debye temperature [42]. Such a relation is based-on the Debye temperature of pure single metals and the molar fraction of each one from:

$$\theta^{-3} = \sum_{i=1}^{n} x_i \, \theta_i^{-3} \quad (5)$$

where θ is the Debye temperature of the alloy (K), x_i is the molar fraction of metal i, and θ_i is the Debye temperature of the pure component i (K). For our Cr-Ta films, it gives rise to the following equation:

$$\theta_{CrTa} = \frac{\theta_{Cr} \times \theta_{Ta}}{\left(x_{Cr} \times \theta_{Cr}^3 + x_{Ta} \times \theta_{Ta}^3\right)^{\frac{1}{3}}} \quad (6)$$

where θ_{CrTa} is the Debye temperature of the Cr-Ta film (K), x_{Cr} is the molar fraction of chromium, and x_{Ta} is the molar fraction of tantalum supposing that $x_{Cr} + x_{Ta} = 1$. Again,

assuming that scattering phenomena of electrons are due to interactions with phonons (at high temperature) and defects (at low temperature), the crossover temperature of Cr-Ta films can be taken as $0.10\times\theta_{CrTa}$ and calculated from equation (6) as a function of Cr-to-Ta atomic concentration ratio, as shown in figure 8b. A good agreement is obtained between experimental values and the Kopp-Neumann relation. This smooth and monotonous behavior of the Debye temperature of alloys as composition changes has ever been reported by others for binary compounds showing a consistency with the Debye temperature predicted by the Kopp-Neumann law [42-46].

For Ta-rich Cr-Ta films, the assumption of the crossover temperature taken as $0.1\times\theta_{Ta}$ is confirmed and for the lowest Cr concentrations, T_{Cr} tends to that of a pure Ta film, *i.e.*, the red dashed line located at 24 K (red opened circle located at [Cr]/[Ta] = 10^{-3} and corresponding to a pure Ta film). Due to the low Debye temperature of Ta (θ_{Ta} = 244 K) and based-on previous investigations showing that the crossover temperature of GLAD Ta films (prepared with α = 80°) is close to that of conventional films [32], one can expect consistent results between measured and calculated crossover temperatures. For Cr-rich Cr-Ta films, the discrepancy between theory and experiment becomes more significant. Calculated T_{Cr} tends to $0.1\times\theta_{Cr}$ = 63 K (blue dashed line) as [Cr]/[Ta] is higher than 10^3, whereas measured T_{Cr} = 70 K (blue opened circle located at [Cr]/[Ta] = 10^3). For such films, one can expect several K of difference, which cannot only be assigned to the experimental errors. Coefficient used to connect crossover and Debye temperatures (*i.e.*, 0.1) has to be adjusted, especially for metals with a high Debye temperature and sputter-deposited with high glancing angles [32]. However, a continuous Debye temperature of Cr-Ta films and so of the crossover temperature *vs.* [Cr]/[Ta] concentration ratio is well obtained from measurements and predicted in a reliable manner assuming a simple additivity relationship based-on Debye temperatures of elementary metals and films composition.

4. Conclusion

Cr-Ta thin films exhibiting a columnar structure are successfully produced by GLAD co-sputter-deposition. Inclination of the columns can be easily and gradually changed by means of simple adjustment of Cr and Ta target currents. For the highest Cr target currents, the typical hcp structure of Cr metal is obtained whereas poorly crystallized films with a mixture of α (bcc structure) and β (tetragonal structure) phases are formed when the Ta target currents predominates. A systematic and opposite variation of both target currents also allows a gradual, symmetric and monotonous evolution of Cr and Ta atomic concentrations, with the deposition of equimolar Cr-Ta films for I_{Cr} = 40 mA and I_{Ta} = 260 mA. This difference between Cr and Ta target current is mainly due to the geometric configuration of the co-sputtering system (higher target-to-substrate distance for Cr than Ta) and because of the highest sputtering yield of Cr compared to that of Ta.

From DC electrical resistivity *vs.* temperature measurements in the range of 7 K to 300 K, scattering mechanisms of electrons are studied and a crossover temperature T_{Cr} is determined as a function of Cr and Ta contents. This temperature corresponds to interferences between electron-phonon and electron-defect interactions. It varies linearly as a function of Cr and Ta target currents and shows a relevant dependence with the Cr-to-Ta atomic concentration ratio. A simple additivity relationship (Kopp-Neumann law) based-on the Debye temperature of pure Cr and Ta metals, and assuming the proportion of each metal was successfully applied to calculate the evolution of the crossover temperature of Cr-Ta films as a function their composition. GLAD co-sputtering of other binary compounds associating two metals with very close Debye temperatures or in the opposite case, with very different Debye temperatures require further investigations in order to check if the Kopp-Neumann relation can be still applied to predict the crossover temperature.

Knowing and understanding the Debye temperature *vs*. composition of thin films made of binary alloys with a columnar structure is of special interest for the development of devices and systems involving materials requiring stable thermal behaviors at the micro- and nanoscales. Other applications based-on the propagation of acoustic waves in MEMS and MOEMS can also be deduced from understanding the electron interactions with phonons and defects assuming electronic transport properties at low temperature.

CRediT authorship contribution statement

Hamidreza Gerami: Data curation; Validation; Writing - review & editing. **Guillem Vilar Soler:** Writing - review & editing. **Jean-Marc Cote:** Data curation; Software; Writing - review & editing. **Jean-Baptiste Sanchez:** Writing - review & editing. **Nicolas Martin:** Writing - review & editing; Supervision; Funding acquisition.

All authors have read and agreed to the published version of the manuscript.

Declaration of Competing Interest

The authors declare that they have no known competing financial interests or personal relationships that could have appeared to influence the work reported in this paper.

Data availability

Data will be made available on request.

Acknowledgements

This work has been achieved in the frame of the EIPHI Graduate school (contract "ANR-17-EURE-0002" and by the Bourgogne-Franche-Comté Region. It has also been partly supported by the French RENATECH network and its FEMTO-ST technological facility.

Appendix A: Supplementary data

Supplementary Material to this article can be found on line at https:// …

References

[1] M. Akiyama, T. Kamohara, K. Kano, A. Teshigahara, Y. Takeuchi, N. Kawahara, Enhancement of piezoelectric response in scandium aluminum nitride alloy thin films prepared by dual reactive cosputtering, Adv. Mater., 21 (2009) 593-596. https://doi.org/10.1002/adma.200802611

[2] B.Y. Oh, J.C. Park, Y.J. Lee, S.J. Cha, J.H. Kim, K.Y. Kim, T.W. Kim, G.S. Heo, Combinatorial study of WInZnO films deposited by rf magnetron co-sputtering, J. Solid State Chem., 184 (2011) 2462-2465. https://doi.org/10.1016/j.jssc.2011.07.024

[3] M. Mazur, J. Domaradzki, D. Wojcieszak, D. Kaczmarek, Investigations of elemental composition and structure evolution in (Ti,Cu)-oxide gradient thin films prepared using (multi)magnetron co-sputtering, Surf. Coat. Technol., 334 (2018) 150-157. https://doi.org/10.1016/j.surfcoat.2017.11.038

[4] M.M. Hawkeye, Brett M.J., Glancing angle deposition: Fabrication, properties, and applications of micro- and nanostructured thin films, J. Vac. Sci. Technol. 25(5) (2007) 1317-1335. https://doi.org/10.1116/1.2764082

[5] S.R. Kennedy, M.J. Brett, O. Toader, S. John, Fabrication of tetragonal square spiral photonic crystals, Nano Lett., 2(1) (2002) 59-62. https://doi.org/10.1021/nl015635q

[6] C. Patzig, T. Karabacak, B. Fuhrmann, V. Rauschenbach, Glancing angle sputter deposited nanostructures on rotating substrates: Experiments and Simulations, J. Appl. Phys., 104 (2008) 094318-9. https://doi.org/10.1063/1.3018145

[7] M.M. Hawkeye, M.T. Taschuk, M.J. Brett, Glancing angle deposition of thin films: Engineering the nanoscale, John Wiley & Son Ltd, Chichester, 2014, https://doi.org/10.1002/9781118847510

[8] S. Hurand, A. Corvisier, B. Lacroix, A.J. Santos, F. Maudet, C. Dupeyrat, R.G. Roja, F.M. Morales, T. Girardeau, F. Paumier, Anisotropic optical properties of indium tin oxide thin films prepared by ion beam sputtering under oblique angle deposition, Appl. Surf. Sci. 595 (2022) 152945-11, https://doi.org/10.1016/j.apsusc.2022.152945

[9] A. Barranco, A. Borras, A.R. Gonzalez-Elipe, A. Palmero, Perspectives on oblique angle deposition of thin films: From fundamentals to devices, Progr. Mater. Sci. 76 (2016) 59-153, https://doi.org/10.1016/j.pmatsci.2015.06.003

[10] S. Mahieu, P. Ghekiere, D. Depla, R. De Gryse, O.I. Lebedev, G. van Tendeloo, Mechanism of in-plane alignment in magnetron sputtered biaxially aligned yttria-stabilized zirconia, J. Crystal Growth 290 (2006) 272-279, https://doi.org/10.1016/j.jcrysgro.2005.12.093

[11] R. Mareus, C. Mastail, F. Nita, A. Michel, G. Abadias, Effect of temperature on the growth of TiN thin films by oblique angle sputter-deposition: A three-dimensional atomistic computational study, Comput. Mater. Sci. 197 (2021) 110662-12, https://doi.org/10.1016/j.commatsci.2021.110662

[12] D.J. Poxson, F.W. Mont, M.F. Schubert, J.K. Kim, E.F. Schubert, Quantification of porosity and deposition rate of nanoporous films grown by oblique-angle deposition, Appl. Phys. Lett. 93 (2008) 101914-3, https://doi.org/10.1063/1.2981690

[13] Q. Xing, J. Ma, C. Wang, Y. Zhang, High-throughput screening solar-thermal conversion films in a pseudobinary (Cr, Fe, V)-(Ta, W) system, ACS Comb. Sci., 20 (2018) 602-610. https://doi.org/10.1021/acscombsci.8b00055

[14] C.M. Müller, A.S. Sologubenko, S.S.A. Gerstl, M.J. Süess, D. Courty, R. Spolenak, Nanoscale Cu/Ta multilayer deposition by co-sputtering on a rotating substrate. Empirical model and experiment, Surf. Coat. Technol., 302 (2016) 284-292. https://doi.org/10.1016/j.surfcoat.2016.06.024

[15] W. Sucharitakul, A. Sukee, P. Leuasoongnoen, M. Horprathum, T. Lertvanithphol, P. Janphuang, P. Mitsomwang, B. Sindhupakorn, Fabrication of an acetone gas sensor based on Si-doped WO_3 nanorods prepared by reactive magnetron co-sputtering with OAD technique, Mater. Res. Express, 8 (2021) 125702-11. https://doi.org/10.1088/2053-1591/ac44d5

[16] R. Kowonga, S. Denchitcharoena, T. Lertvanithpholb, N. Triamnakc, C. Chananonnawathornb, K. Jaruwongrungseeb, A. Klamchuend, P. Muthitamongkole, W. Phae-ngamf, H. Nakajimag, P. Songsiriritthigulg,h, M. Horprathum Nanostructure optimization of Zr-W-Ti metallic glass thin films via multitarget co-sputtering with oblique angle deposition approach, J. Alloy. Compd., 886 (2021) 161265-9. https://doi.org/10.1016/j.jallcom.2021.161265

[17] T. Zhang, C. Zeng, Y. Xia, H. Zhang, B. Suna, H. Wang, Y. Zhao, Morphology evolution and photocatalytic applications of W-doped Bi_2O_3 films prepared using unique oblique angle co-sputtering technology, Ceram. Int., 45 (2019) 21968-7. https://doi.org/10.1016/j.ceramint.2019.07.211

[18] W. Phae-ngam C. Chananonnawathorn, T. Lertvanithphol, B. Samransuksamer, M. Horprathum, T. Chaiyakun, Effect of the deposition time on nanocolumnar TiZrN films grown by reactive magnetron co-sputtering with OAD technique, Mater. Tehnol., 55 (2021) 65-70. https://doi.org/10.17222/mit.2019.189

[19] Y. Motemani, C. Khare, Alan Savan, M. Hans, A. Paulsen, J. Frenzel, C. Somsen, F. Mücklich, G. Eggeler, A. Ludwig, Nanostructured Ti–Ta thin films synthesized by combinatorial glancing angle sputter deposition, Nanotechnology, 27 (2016) 495604-14. https://doi.org/10.1088/0957-4484/27/49/495604

[20] C. Sparcher, C. Lopes, C. Gabor, D. Munteanu, M. Correa, F. Vaz, A. Ferreira, Characterization of GLAD-grown TiCu thin films for thermo-resistive sensing applications, Sens. Actuator A-Phys., 376 (2024) 115661-8. https://doi.org/10.1016/j.sna.2024.115661

[21] U. Waiwijit, C. Chananonnawathorn, P. Eimchai, T. Bora, G.L. Hornyak, N. Nuntawong, Fabrication of Au-Ag nanorod SERS substrates by co-sputtering technique and dealloying with selective chemical etching, Appl. Surf. Sci., 530 (2020) 147171-9. https://doi.org/10.1016/j.apsusc.2020.147171

[22] C. Wattanawikkam, A. Bootchanont, P. Porjai, C. Jetjamnong, R. Kowong, T. Lertvanithphol, C. Chananonnawathorn, P. Chirawatkul, N. Chanlek, H. Nakajima, P. Songsiriritthigul, N. Kiama, W. Nareejun, P. Tomkham, C. Ponchio, S. Rahong, A. Klamchuen, M. Horprathum, Phase evolution in annealed Ni-doped WO_3 nanorod films prepared via a glancing angle deposition technique for enhanced photoelectrochemical performance, Appl. Surf. Sci., 584 (2022) 152581-10. https://doi.org/10.1016/j.apsusc.2022.152581

[23] M. Zhou, D. Gall, Two-Component Nanorod Arrays by Glancing-Angle Deposition, Small, 4(9) (2007) 1351-1354. https://doi.org/10.1002/smll.200701289

[24] C.M. Zhou, H.F. Li, D. Gall, Multi-component nanostructure design by atomic shadowing, Thin Solid Films, 517 () 1214-1218. https://doi.org/10.1016/j.tsf.2008.05.049

[25] P. Pedrosa, A. Ferreira, N. Martin, M. Arab Pour Yazdi, A. Billard, S. Lanceros-Mendez, F. Vaz, Nanosculptured Janus-like TiAg thin films obliquely deposited by GLAD co-sputtering for temperature sensing, Nanotechnology, 29 (2018) 355706-11. https://doi.org/10.1088/1361-6528/aacba8

[26] R. El Beainou, J.M. Cote, V. Potin, N. Martin, Contrasted morphologies in nanostructured Janus W-Cu columns, Materials Today Communications, 27 (2021) 102331-4. https://doi.org/10.1016/j.mtcomm.2021.102331

[27] H. Boukhalfa, V. Potin, N. Martin, Ballistic and thermalized regimes to tune structure and conducting properties of W-Mo thin films, Vacuum, 204 (2022) 111347-10. https://doi.org/10.1016/j.vacuum.2022.111347

[28] H. Boukhalfa, V. Potin, N. Martin, Microstructural analysis and electrical behaviours of co-sputtered W-Ag thin films with a tilted columnar architecture, J. Phys. D: Appl. Phys., 54 (2021) 255304-9. https://doi.org/10.1088/1361-6463/abf312

[29] N. Martin, J.M. Cote, H. Boukhalfa, V. Potin, Checkerboard-like structure in columnar W-Mo thin films, Funct. Mater. Lett., 15 (6) (2022) 2251043-5. https://doi.org/10.1142/s1793604722510432

[30] A. Chargui, R. El Beainou, A. Mosset, S. Euphrasie, V. Potin, P. Vairac, N. Martin, Influence of thickness and sputtering pressure on electrical resistivity and elastic wave propagation in oriented columnar tungsten thin films, Nanomaterials, 10(1) 81 (2020) 1-18. https://doi.org/10.3390/nano10010081

[31] R. El Beainou, R. Salut, L. Robert, J.M. Cote, V. Potin, N. Martin, Anisotropic conductivity enhancement in inclined W-Cu columnar films, Mater. Lett., 232 (2018) 126-129. https://doi.org/10.1016/j.matlet.2018.08.120

[32] H. Gerami, J.M. Cote, A.J. Santos, N. Martin, Low temperature dependence of electrical resistivity in obliquely sputter-deposited transition metal thin films, Surf. Interfaces, 54 (2024) 105113-11. https://doi.org/10.1016/j.surfin.2024.105113

[33] R. El Beainou, A. Chargui, P. Pedrosa, A. Mosset, S. Euphrasie, P. Vairac, N. Martin, Electrical conductivity and elastic wave propagation anisotropy in glancing angle deposited tungsten and gold films, Appl. Surf. Sci., 475 (2019) 606-614. https://doi.org/10.1016/j.apsusc.2019.01.041

[34] D. Vick, T. Smy, M.J. Brett, Growth behavior of evaporated porous thin films, J. Mater. Res., 17(11) (2002) 2904-2911. https://doi.org/10.1557/jmr.2002.0421.

[35] N. Martin, J. Sauget, T. Nyberg, Anisotropic electrical resistivity during annealing of oriented columnar titanium films, Mater. Lett., 105 (2013) 20-23. https://doi.org/10.1016/j.matlet.2013.04.058.

[36] S.Y. Davydov, Calculation of the activation energy for surface self-diffusion of transition-metal atoms, Physics of Solid State, 41(1) (1999) 8-10. https://doi.org/10.1134/1.1130717

[37] R. Alvarez, J.M. García-Martín, M. Macías-Montero, L. Gonzalez-Garcia, J.C. González, V. Rico, J. Perlich, J. Cotrino, A.R. González-Elipe , A. Palmero, Growth regimes of porous gold thin films deposited by magnetron sputtering at oblique incidence: from compact to columnar microstructures, Nanotechnology 24 (2013) 45604-9. https://doi.org/10.1088/0957-4484/24/4/045604

[38] J.J. Colin, G. Abadias, A. Michel, C. Jaouen, On the origin of the metastable β-Ta phase stabilization in tantalum sputtered thin films, Acta Mater., 126 (2017) 481-493. https://doi.org/10.1016/j.actamat.2016.12.030

[39] J. Peralta, J. Esteve, A. Lousa, δ-A15 and bcc phases coexist in sputtered chromium coatings with moderate oxygen contents, Thin Solid Films, 293 (2020) 137676-135677. https://doi.org/10.1016/j.tsf.2019.137676

[40] R. El Beainou, N. Martin, V. Potin, P. Pedrosa, M. Arab Pour Yazdi, A. Billard, Correlation between structure and electrical resistivity of W-Cu thin films prepared by GLAD co-sputtering, Surf. Coat. Technol., 313 (2017) 1-7. https://doi.org/10.1016/j.surfcoat.2017.01.039

[41] N. Matsunami, Y. Yamamura, Y. Itikawa, N. Itoh, Y. Kazumata, S. Miyagawa, K. Morita, R. Shimizu, and H. Tawara, Energy dependence of the ion-induced sputtering yields of

monatomic solids, Atom. Data Nucl. Data Tables, 31(1) (1984) 1-80. https://doi.org/10.1016/0092-640x(84)90016-0

[42] N.T. Hong, H.K. Hieu, Investigation of Debye temperature and thermal disorder in Fe-Cr intermetallic alloys, Phys. Scr., 96 (2021) 075701-8. https://doi.org/10.1088/1402-4896/abf791

[43] S.M. Dubiel, J. Cieslak, B.F.O. Costa, Debye temperature of disordered bcc-Fe-Cr alloys, J. Phys.: Condens. Matter, 22 (2010) 055402-6. https://doi.org/10.1088/0953-8984/22/5/055402

[44] K. Wang, D. Du, B. Chang, Y. Hong, J. Ju, S. Sun, H. Fu, Mechanical properties, electronic structures, and Debye temperature of Ni_xB_y compounds obtained by the first principles calculations, Crystals, 8 (2018) 451-13. https://doi.org/10.3390/cryst8120451

[45] H.M. Kagaya, E.I. Serita, M. Sato, T. Soma, Lattice dynamics and Debye temperature of Al-Cu, Al-Si and Al-Ge alloy systems, Solid State Commun., 100(10) (1996) 727-730. https://doi.org/10.1016/0038-1098(96)00388-2

[46] L.D. Geoffrion, G. Guisbiers, Physico-chemical properties of selenium-tellurium alloys across the scales, Nanoscale Adv., 3 (2021) 4254-4270. https://doi.org/10.1039/d1na00087j

Figure captions

Figure 1:

Schematic representation of the oblique angle co-sputtering system implemented to deposit Cr-Ta thin films. Each target is tilted with the same deposition angle, *i.e.*, $\alpha_{Cr} = \alpha_{Ta} = 80°$. The target-to-substrate distances are maintained at 65 mm for Cr and 95 mm for Ta. The substrate is fixed (no rotation following ϕ angle) and both targets are focused on the center of the substrate position ($x = 0$ mm).

Figure 2:

Scanning electron microscopy (SEM) observations of top and cross-section views of co-deposited Cr-Ta films with various Cr and Ta target currents (I_{Cr}/I_{Ta}). They are systematically and inversely changed from 0 to 300 mA. Column apexes and tilts can be adjusted as a function of both target currents. Arrows indicate the incoming of Cr (blue) and Ta (red) particle fluxes.

Figure 3:

GIXRD patterns of Cr-Ta thin films co-sputter-deposited on glass substrate by oblique angle deposition. Cr and Ta target currents are systematically and inversely changed from 0 to 300 mA. Occurrence of the hcp Cr phase and α and/or β-Ta phases depends on the Cr and Ta target currents.

Figure 4:

Cr-to-Ta atomic concentration ratio [Cr]/[Ta] as a function of the position x on the Si(100) substrate and for different current intensities of chromium and tantalum targets. Measurements of the atomic concentration are performed on seven different locations. The center of the substrate corresponds to x = 0 mm, x = −6 mm is the left-hand side (close to the chromium target) and x = +6 mm is the right-hand side (close to the tantalum target).

Figure 5:

Cr and Ta atomic concentrations as a function of Cr and Ta target currents of 400 nm thick Cr-Ta thin films co-sputter-deposited by GLAD on Si(100). A symmetric, reverse and continuous evolution of each metal concentration is produced with equimolar films obtained for I_{Cr} = 40 mA and I_{Ta} = 260 mA.

Figure 6:

DC electrical resistivity ρ *vs.* temperature T of Cr-Ta thin films sputter-deposited on glass. Cr and Ta target currents I_{Cr} and I_{Ta}, are systematically and reversely changed from 0 to 300 mA. I_{Cr}/I_{Ta} = 300/0 mA corresponds to pure Cr film, whereas I_{Cr}/I_{Ta} = 0/300 mA relates to pure Ta film.

Figure 7:

Resistivity *vs.* temperature of a Cr-Ta film prepared by oblique angle co-sputtering with I_{Cr} = 200 mA and I_{Ta} = 100 mA. The crossover temperature T_{Cr} = 44 K representing the transition from T-linear to T^5 behavior is determined taking into account the intersection between the

residual resistivity (resistivity value at 7 K, namely ρ_{7K}, which is temperature independent), and the derivative of the resistivity by temperature at 100 K, $(d\rho/dT)_{100K}$.

Figure 8:

a) Crossover temperature T_{Cr} as a function of Cr and Ta target currents I_{Cr} and I_{Ta}, respectively. Cr and Ta Debye temperatures, namely θ_{Cr} and θ_{Ta}, respectively, are also indicated. Green solid line is a plot from equation (2) of the crossover temperature T_{Cr} *vs.* target current I_{Cr} assuming $0.1\times\theta_{Cr}$ and $0.1\times\theta_{Ta}$ as boundaries for pure Cr (I_{Cr}/I_{Ta} = 300/0 mA) and Ta (I_{Cr}/I_{Ta} = 0/300 mA). Black solid line is a linear fit from experimental crossover temperatures. b) Evolution of the crossover temperature T_{Cr} as a function of Cr-to-Ta atomic concentration ratio. Blue dashed line is $0.1\times\theta_{Cr}$, red dashed line is $0.1\times\theta_{Ta}$, and green line is one-tenth of Debye temperature $\theta_{Cr\text{-}Ta}$ of Cr-Ta films calculated from equation (6).